JACS
JOURNAL OF THE AMERICAN CHEMICAL SOCIETY
Article
pubs.acs.org/JACS

Surface Composition Tuning of Au–Pt Bimetallic Nanoparticles for Enhanced Carbon Monoxide and Methanol Electro-oxidation

Jin Suntivich,[†,▽] Zhichuan Xu,[‡,▽] Christopher E. Carlton,[‡] Junhyung Kim,[‡] Binghong Han,[†] Seung Woo Lee,[‡] Nicéphore Bonnet,[†] Nicola Marzari,[†,¶] Lawrence F. Allard,[⊥] Hubert A. Gasteiger,*[,‡,∥] Kimberly Hamad-Schifferli,*[,‡,§] and Yang Shao-Horn*[,†,‡]

[†]Department of Materials Science and Engineering, [‡]Department of Mechanical Engineering, and [§]Department of Biological Engineering, Massachusetts Institute of Technology, 77 Massachusetts Avenue, Cambridge, Massachusetts 02139, United States

[⊥]Microscopy Group, Oak Ridge National Laboratory, 1 Bethel Valley Road, Building 4515, Oak Ridge, Tennessee 37831, United States

Supporting Information

ABSTRACT: The ability to direct bimetallic nanoparticles to express desirable surface composition is a crucial step toward effective heterogeneous catalysis, sensing, and bionanotechnology applications. Here we report surface composition tuning of bimetallic Au–Pt electrocatalysts for carbon monoxide and methanol oxidation reactions. We establish a direct correlation between the surface composition of Au–Pt nanoparticles and their catalytic activities. We find that the intrinsic activities of Au–Pt nanoparticles with the same bulk composition of $Au_{0.5}Pt_{0.5}$ can be enhanced by orders of magnitude by simply controlling the surface composition. We attribute this enhancement to the weakened CO binding on Pt in discrete Pt or Pt-rich clusters surrounded by surface Au atoms. Our finding demonstrates the importance of surface composition control at the nanoscale in harnessing the true electrocatalytic potential of bimetallic nanoparticles and opens up strategies for the development of highly active bimetallic nanoparticles for electrochemical energy conversion.

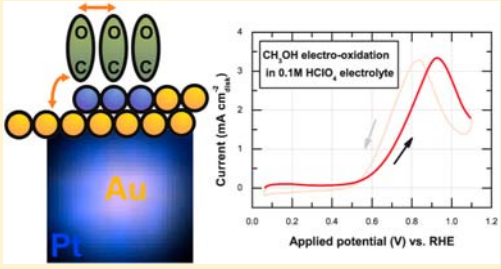

INTRODUCTION

Fundamental studies on extended surfaces have shown that the activity of an electrocatalyst can be described by its surface electronic structure, which, if properly controlled, can radically enhance the electrocatalytic activity.[1−5] However, realization of this enhancement in nanomaterials has been challenging because of the difficulty in controlling surface composition at the nanoscale. As precise control over surface composition is critical to obtain the most optimum surface electronic structure and catalytic activity,[1,3,6] mastering the ability to control surface composition for nanoparticles is a critical step toward applications in fuel cells based on small molecules of energy consequence such as methanol and natural gas derivatives. Toward this end, methods to precisely control surface chemistry at the nanoscale including selective leaching,[2,7] adsorbate-driven segregation,[8−12] and multistep synthesis[13,14] have been developed. However, a direct correlation between tailored surface compositions of nanoparticles and their catalytic activities, particularly in a low pH environment mimicking a proton-exchanged membrane electrolyte, still remains elusive due to the fact that only a few metals are stable in acid and that a very limited number of techniques can allow quantification of surface compositions of nanoparticles.[2,7] In this contribution, we accomplish the surface composition control by strategically selecting Au–Pt chemistry as both Au and Pt are stable in acid and can be quantified electrochemically (vide infra). By tuning the surface composition of Au–Pt nanoparticles, we establish a direct correlation between surface compositions and catalytic activities of Au–Pt nanoparticles for the CO electro-oxidation reaction (COR: $CO + H_2O \rightarrow CO_2 + 2H^+ + 2e^-$) and methanol electro-oxidation reaction (MOR: $CH_3OH + H_2O \rightarrow CO_2 + 6H^+ + 6e^-$). We find that the intrinsic activities of Au–Pt nanoparticles with a bulk nanoparticle composition of $Au_{0.5}Pt_{0.5}$ can be enhanced by at least an order of magnitude by simply controlling the surface composition, thereby demonstrating the importance of surface composition control for energy conversion nanomaterials.

Au–Pt nanoparticles have been the subject of many electrocatalytic studies such as O_2 reduction reaction,[15,16] MOR,[17,18] and COR.[13] In bulk, Au and Pt are immiscible, but at nanoscale, the two elements can alloy and undergo solid solutioning.[19] In this study, we utilize this phenomenon to synthesize single-phase $Au_{0.5}Pt_{0.5}$ nanoparticles. We then control the $Au_{0.5}Pt_{0.5}$ nanoparticles to have surface Pt or Au enrichment by taking advantage of the difference in the surface free[20] and binding energies with various adsorbates between Pt and Au.[21] The degree of surface Pt or Au enrichment is quantified by element-specific surface electro-adsorption/desorption via cyclic voltammetry and energy-dispersive

Received: February 26, 2013
Published: May 6, 2013

   dx.doi.org/10.1021/ja402072r | J. Am. Chem. Soc. 2013, 135, 7985−7991

spectroscopy (EDS) in an aberration-corrected scanning transmission electron microscope (STEM). We show that Au enrichment on the surface greatly enhances the intrinsic activities of the Au−Pt nanoparticles for COR by orders of magnitude in comparison to commercial Pt and Au nanoparticles. For MOR, Au−Pt nanoparticles with a surface Pt composition of ∼70 atom % have the maximum MOR activity, comparable to state-of-the-art Pt-alloy nanoparticle catalysts. The activity enhancement of Au−Pt nanoparticles in catalyzing COR and MOR is attributed to the weakening of the CO binding on Pt following formation of a discrete Pt or Pt-rich cluster surrounded by Au atoms.

EXPERIMENTAL SECTION

Nanoparticle Synthesis and Catalyst Preparation. Amounts of 0.25 mmol of $HAuCl_4$ (Sigma-Alrich) and 0.25 mmol of H_2PtCl_6 (Sigma-Alrich) were dissolved in 20 mL of oleylamine (Sigma-Alrich) at 40 °C under an Ar blanket. The solution was evaporated and heat-treated at 160 °C for 2 h. Afterward, 100 mL of ethanol was added, and the mixture was centrifuged at 6000 rpm for 10 min. The sediments were redispersed and ultrasonicated in a mixture of 600 mL of hexane and ∼320 mg of Vulcan XC-72 (Premetek, USA). Afterward, the solution-containing supported $Au_{0.5}Pt_{0.5}$ nanoparticles were purged with Ar at room temperature and then dried in vacuum for 24 h. Procedures for sequential loading Au−Pt nanoparticles on Vulcan carbon (21 wt %) and thermal treatments are detailed in the Supporting Information.

Scanning Transmission Electron Microscopy-Energy-Dispersive X-Ray Spectroscopy (STEM-EDS). A JEOL JEMS2200 STEM outfitted with a CEOS aberration corrector and a Bruker XFlash 5030 T detector at the Advanced Microscopy Laboratory at the Oak Ridge National Laboratory was used to form conventional bright and dark field images, as well as EDX maps as part of the SHaRE user program. All imaging and spectroscopy was done at 200 KeV. The EDS maps were formed with acquisition times of ≥20 min utilizing drift correction and were postprocessed with a smooth algorithm (Bruker Espirit). The effect of the smoothing algorithm is shown in Supporting Information Figure S11. We note that the surface composition as evaluated by STEM-EDS does not precisely match with the result from CV; this is likely a result of the resolution limit of STEM-EDS, which was estimated to be ∼0.5 nm, approximately twice the distance between two (111) planes.[22] An additional STEM-EDS image is included in the Supporting Information.

Electrochemical Characterization. The thin-film rotating disk electrode for the $Au_{0.5}Pt_{0.5}$ nanoparticle study was a drop cast from a solution containing the catalyst and an appropriate amount of Nafion (ion power) with a final composition of 18 μg_{Au+Pt} cm^{-2}_{disk}, 68 μg_{Vulcan} cm^{-2}_{disk}, and 38 μg_{Nafion} cm^{-2}_{disk}. Electrochemical measurements were conducted with a rotating-disk electrode using a bipotentiostat (Pine). The electrolyte was prepared using a dilution of either H_2SO_4 (Fluka) or $HClO_4$ (GFS Chemicals) using Milli-Q water (18 MΩ·cm). The potential range for both COR and MOR studies was restricted between 0.05 and 1.1 V vs RHE. Error bars represent standard deviations from at least three independent measurements.

RESULTS AND DISCUSSION

Tuning the Surface Composition of $Au_{0.5}Pt_{0.5}$ Nanoparticles. We synthesized four different $Au_{0.5}Pt_{0.5}$ nanoparticles with surface atomic compositions ranging from ∼90 to ∼10 atom % Pt (Figure 1). First, $Au_{0.5}Pt_{0.5}$ nanoparticles were synthesized by a colloidal route as demonstrated previously,[23] which yielded AuPt particles with Pt-enriched surface and a nominal bulk composition of $Au_{0.5}Pt_{0.5}$, as revealed by inductive plasma coupling. We then induced surface Au enrichment using the fact that Au has a lower surface energy than Pt[20,24] by heat-treating as-synthesized $Au_{0.5}Pt_{0.5}$ nanoparticles supported on carbon (21 wt. % $Au_{0.5}Pt_{0.5}$/C) in Ar at

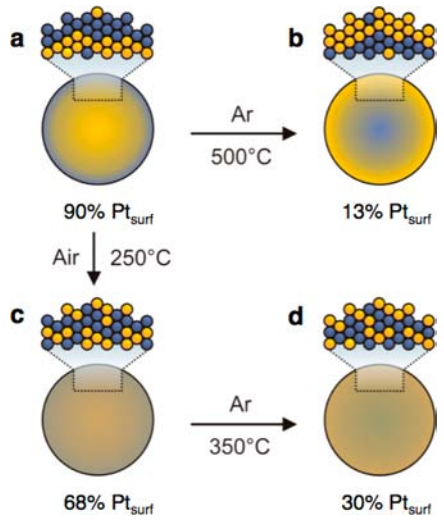

Figure 1. Schematic models of $Au_{0.5}Pt_{0.5}$ nanoparticles undergoing surface-energy-driven restructuring upon different thermal treatments. Differential surface energies of Au and Pt in different environments enable adsorbate-driven segregation, which leads to different surface compositions despite all having the same bulk composition.

500 °C (Figure 1a and 1b), during which an average particle size grew from ∼6 to ∼8 nm (Supporting Information, Figure S1) and no phase separation was detected by XRD (Supporting Information, Figure S2). The surface composition change from Pt-rich to Au-rich was evaluated using element-specific surface electro-adsorption/desorption via cyclic voltammetry (CV) and aberration-corrected EDS in STEM. Using the charge associated with the hydrogen adsorption/desorption and the Au oxide reduction in the CV data, the Pt and Au surface compositions were extracted, respectively (Supporting Information, Figure S3). Specifically, upon heating at 500 °C in air (Figure 1a and 1b), Pt-rich (90 ± 3 atom % Pt) surfaces of colloidal $Au_{0.5}Pt_{0.5}$ nanoparticles were changed to a Au-rich surface (88 ± 1 atom % Au). This change in the surface composition was further confirmed by STEM-EDS analysis of Pt and Au distributions within individual $Au_{0.5}Pt_{0.5}$ nanoparticles. Specifically, a Pt shell (blue) and Au core (yellow) were found for colloidal $Au_{0.5}Pt_{0.5}$ nanoparticles (Figure 3a), while a Au shell and Pt were observed for $Au_{0.5}Pt_{0.5}$ nanoparticles after the 500 °C heat treatment in Ar in Figure 3b. Additional representative TEM images are included in the Supporting Information.

$Au_{0.5}Pt_{0.5}$ nanoparticles with ∼70 and ∼30 atom % Pt on the surface were also obtained by heat-treating as-synthesized $Au_{0.5}Pt_{0.5}$ nanoparticles supported on carbon (Figure 1c and 1d) at temperature lower than 500 °C. A treatment at 250 °C in air gave rise to a 66 ± 4 atom % Pt surface from CV measurements (Figure 2c), in good agreement with the STEM-EDS analysis of Pt and Au distributions within individual particles (Figure 3c). We note that this condition (250 °C in air) represents the lower limit of the heat-treating temperatures for surface Au enrichment, where the majority of surfactant molecules that stabilize Pt on the surface must be removed to allow Au to migrate and enrich the surface. In comparison, the heat treatment at 250 °C in Ar did not result in any measurable change in the surface composition (Supporting Information, Figure S4a) because fewer surfactant molecules were removed during heating in Ar than in air. This hypothesis is supported by the thermal gravimetric analysis data, where more weight loss

dx.doi.org/10.1021/ja402072r | J. Am. Chem. Soc. 2013, 135, 7985−7991

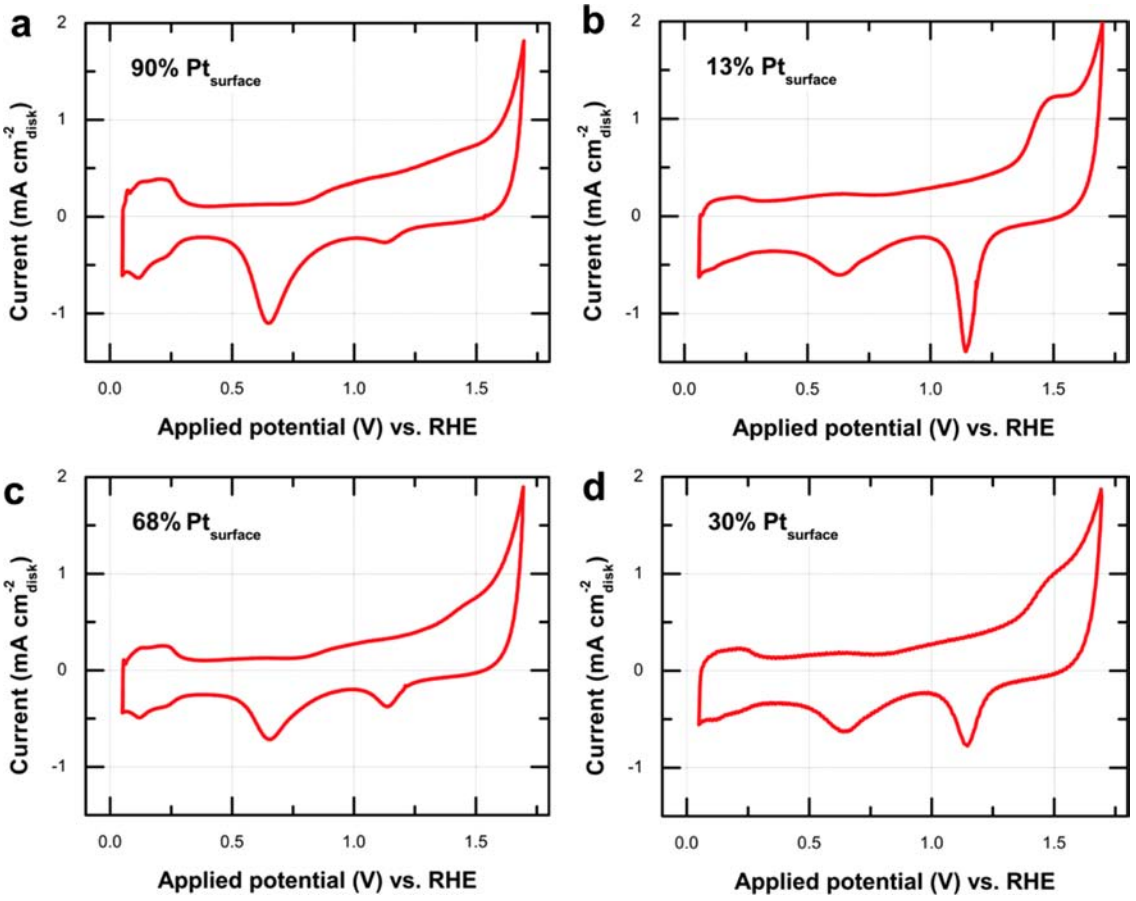

Figure 2. Cyclic voltammograms of $Au_{0.5}Pt_{0.5}$ nanoparticles in 0.5 M H_2SO_4 at 50 mV/s scan rate. (a) As-synthesized $Au_{0.5}Pt_{0.5}$ (90 ± 3% surface Pt), (b) Ar treatment at 500 °C for 30 min (13 ± 5% surface Pt), (c) air treatment at 250 °C for 30 min (68 ± 3% surface Pt), and (d) air treatment at 250 °C for 30 min, followed by Ar treatment at 350 °C for 30 min (30 ± 1% surface Pt). Standard deviations were calculated form three independent measurements.

was found for $Au_{0.5}Pt_{0.5}$ nanoparticles following the heat treatment in Ar than in air at 250 °C (Supporting Information, Figure S4b). Additionally, a subsequent heat treatment in Ar at 350 °C gave rise to further surface Au enrichment, yielding a 28 ± 1 atom % Pt surface concentration (Figure 2d) as measured using CV and confirmed by spectral Pt and Au maps from the EDS analysis (Figure 3d). We point out that, because the 30 atom % Pt particle preparation requires a two-step heat treatment, dealloying of Pt and Au can begin to occur, as can be seen via TEM (Figure 3d). It also should be mentioned that some differences may exist in the surface Pt and Au concentrations as quantified via CV and EDS measurements as EDS in the STEM with spatial resolution of 0.5 nm is less sensitive to the topmost layer of $Au_{0.5}Pt_{0.5}$ nanoparticles than CV measurements.[22]

CO Electro-Oxidation on $Au_{0.5}Pt_{0.5}$ Nanoparticles in Acid. The CO oxidation current was obtained from scanning a thin film of $Au_{0.5}Pt_{0.5}$ nanoparticles deposited on a rotating disk electrode (RDE) in a CO-saturated $HClO_4$ solution as a function of potential. Geometric current densities (current normalized to the RDE area) of the $Au_{0.5}Pt_{0.5}$ nanoparticles with different surface compositions (Figure 4a) showed that increasing the surface Au concentration enhanced the intrinsic activity of COR with $Au_{0.5}Pt_{0.5}$ nanoparticles with ∼10 and ∼30 atom % Pt surface exhibiting specific activities (current normalized to the combined electrochemical active surface area of Pt and Au) markedly higher than those with ∼70 and ∼90 atom % Pt by 1 order of magnitude and commercial Au/C and Pt/C (Tanaka Kikinzoku, "TKK") by 2 orders of magnitude (see Figure 4b and Supporting Information, Figure S5). The enhancement in the specific activity was also observed at the mass level, where the mass activities for $Au_{0.5}Pt_{0.5}$ nanoparticles with ∼10 and ∼30 atom % Pt on the surface were found to be significantly higher than those with ∼70 and ∼90 atom % Pt and commercial Au/C and Pt/C (Supporting Information, Figure S6).

We hypothesize the enhancement in the CO electro-oxidation kinetics of $Au_{0.5}Pt_{0.5}$/C to stem from the modified electronic structure of surface Pt that is surrounded by Au neighbors,[25] which results in a weakened binding strength of CO_{ad}. This hypothesis is supported by the recent single-crystal work, whereby isolated surface Pt clusters surrounded by Au neighbors (see Supporting Information, Scheme S1) were shown to have weaker CO binding than Pt due to lateral interactions and the absence of binding contribution from the next nearest Pt atoms.[25,26] We believe that this configuration, where the Pt or Pt-rich clusters are surrounded by Au or Au-rich atoms, well represents the surface structure of our $Au_{0.5}Pt_{0.5}$ nanoparticles with surface Au enrichment as Pt prefers to have Pt as its nearest neighbor due to favorable enthalpy of the Pt−Pt bond.[27] Further evidence on the importance of weakened CO_{ad} binding came from a positive reaction order of CO concentration on the COR activity observed for $Au_{0.5}Pt_{0.5}$ nanoparticles with 30% surface Pt and a

dx.doi.org/10.1021/ja402072r | J. Am. Chem. Soc. 2013, 135, 7985−7991

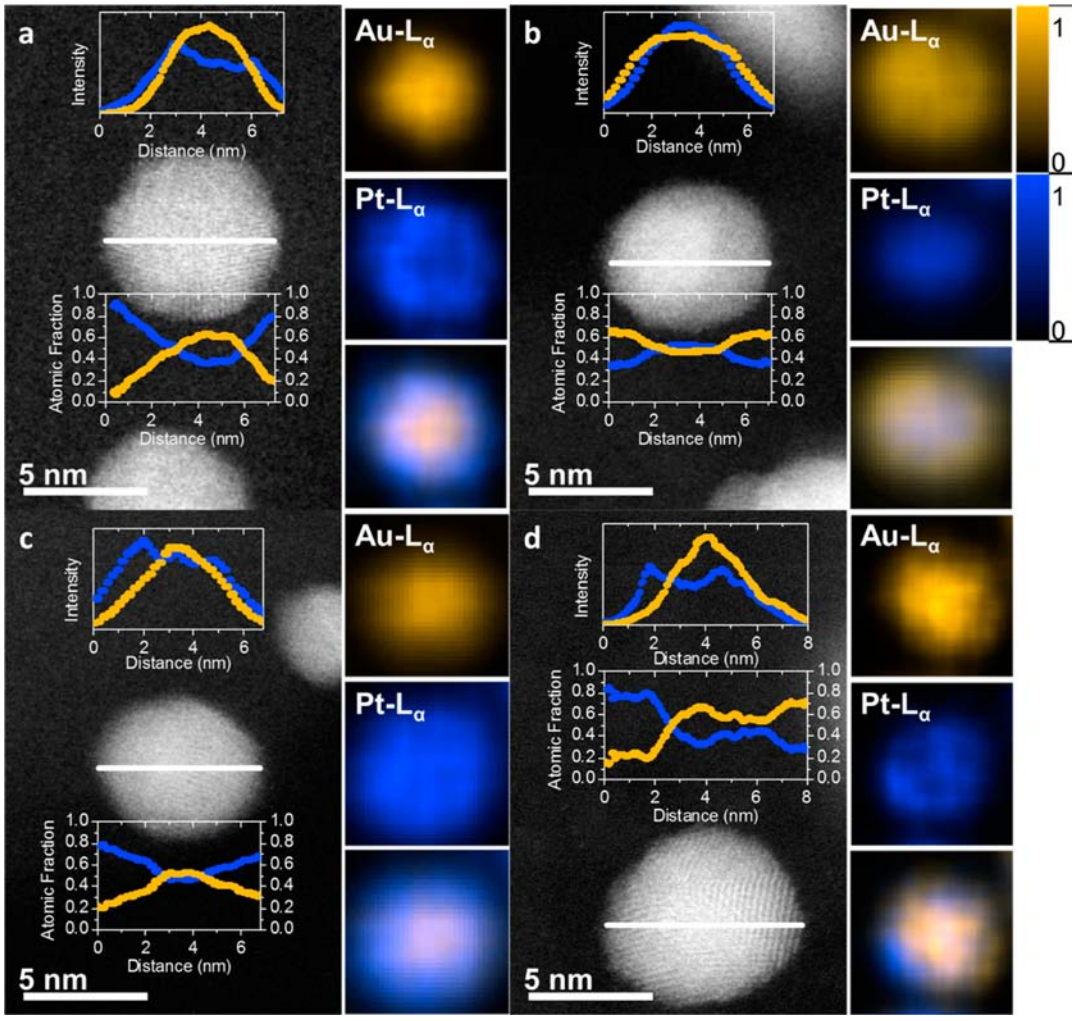

Figure 3. Aberration-corrected scanning transmission electron microscopy-energy-dispersive X-ray spectroscopy (STEM-EDS) of $Au_{0.5}Pt_{0.5}$ nanoparticles. (a) As-synthesized $Au_{0.5}Pt_{0.5}$ (90% surface Pt), (b) Ar treatment at 500 °C for 30 min (13% surface Pt), (c) air treatment at 250 °C for 30 min (68% surface Pt), (d) air treatment at 250 °C for 30 min, followed by Ar treatment at 350 °C for 30 min (30% surface Pt). The signal count from the trace line is shown in the top inset, showing Pt and Au L_α and, in the bottom inset, their calculated relative concentrations. The right panel shows Pt, Au, and their combined L_α mappings. The intensity plots are based on a raw EDS signal that was smoothed in a manner detailed by Figure S10 (Supporting Information). The colors of the maps were universally scaled so that the color scale of 1 represents 10% less than the maximum concentration of either Pt or Au in any of the nanoparticles. Signal processing procedures and additional representative TEM images are included in the Supporting Information.

zero reaction order (invariant activity with CO concentration) for ~70 atom % Pt (Supporting Information, Figure S7). This finding is in contrast to the case of Pt/C, which has a negative reaction order, indicative of the poisonous nature of CO for COR.[28]

We rule out the possibility that CO may adsorb on Au because the CO stripping charge scales with Pt instead of the total surface area (see Supporting Information, Figure S8) and that Au is known to undergo CO desorption below room temperature in the form of either extended[29] or Au−Pt alloy surfaces.[26,30] As we did not observe significant differences in the surface atomic structure after different heat treatments (see Supporting Information Figure S9 and Table S1), we also rule out the possibility that the enhanced COR kinetics stem from $Au_{0.5}Pt_{0.5}$ nanoparticles with different surface facets, in particular, high-index planes. We therefore propose that the enhancement comes from the intrinsic electronic structure modification on Pt by Au. In this hypothesis, Au serves to modify Pt electronic structure and thereby to more accurately assess the catalytic trend, and we compare the COR activity normalized by the Pt surface area (Figure 4b, blue, right axis). We find that the COR activity monotonically increases with Au content, consistent with the continuing decrease in the CO adsorption energy with increasing Au concentration, in agreement with the literature.[26] The critical role of CO binding strength in the COR kinetics can be understood using the framework of the well-known Langmuir−Hinshelwood mechanism, where $CO_{ad} + OH_{ad} \rightarrow COOH_{ad}$ is the rate-limiting step.[31,32] Specifically, weakened CO binding on Pt reduces Pt poisoning, which decreases CO coverage and allows OH to nucleate more efficiently, and the activation energy, which is prohibitively high as a result of strongly adsorbed CO_{ad} on Pt, consequently enhancing the COR kinetics.

Methanol Electro-Oxidation on $Au_{0.5}Pt_{0.5}$ Nanoparticles in Acid. We further applied the thin-film RDE methodology to examine the MOR activities of $Au_{0.5}Pt_{0.5}$ nanoparticles (Figures 5a,b). Methanol oxidation currents normalized to the combined electrochemically active surface

dx.doi.org/10.1021/ja402072r | J. Am. Chem. Soc. 2013, 135, 7985−7991

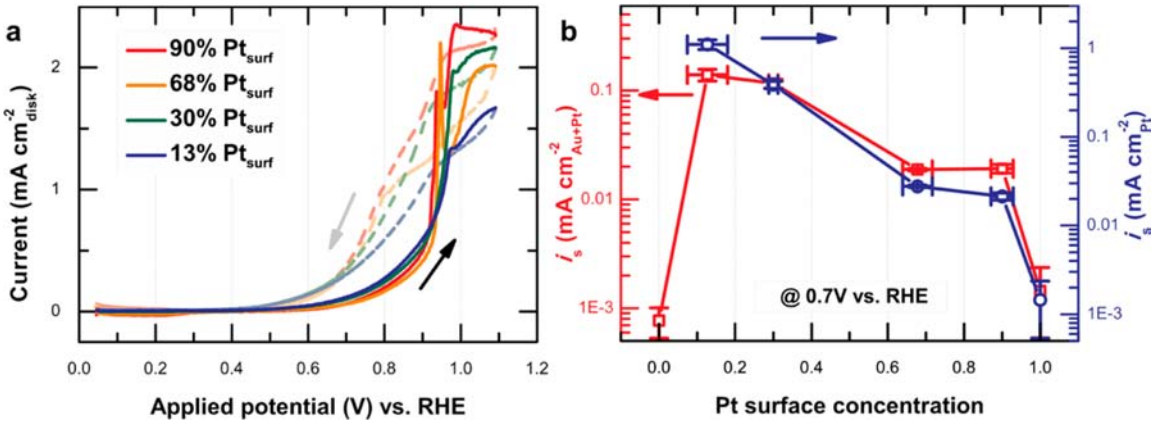

Figure 4. Activities of $Au_{0.5}Pt_{0.5}$ NPs at various surface compositions for carbon monoxide electro-oxidation reaction (COR). (a) As-measured COR current densities of $Au_{0.5}Pt_{0.5}$ NPs at various surface compositions in 0.1 M $HClO_4$ (measured at 1600 rpm, 5 mV s^{-1} scan rate, 0.018 mg_{metal} cm^{-2}_{disk} loading). (b) The specific COR activities, i_s, $Au_{0.5}Pt_{0.5}$ NPs (capacitance-corrected) normalized to either both Pt and Au surface area (red, left axis) or Pt surface area (blue, right axis) from a positive-going scan direction as a function of surface composition at 0.7 V vs RHE potential. The activity for 100% Pt was obtained from commercial Pt/C catalyst (Tanaka Kikinzoku). Error bars represent standard deviations of at least three independent measurements.

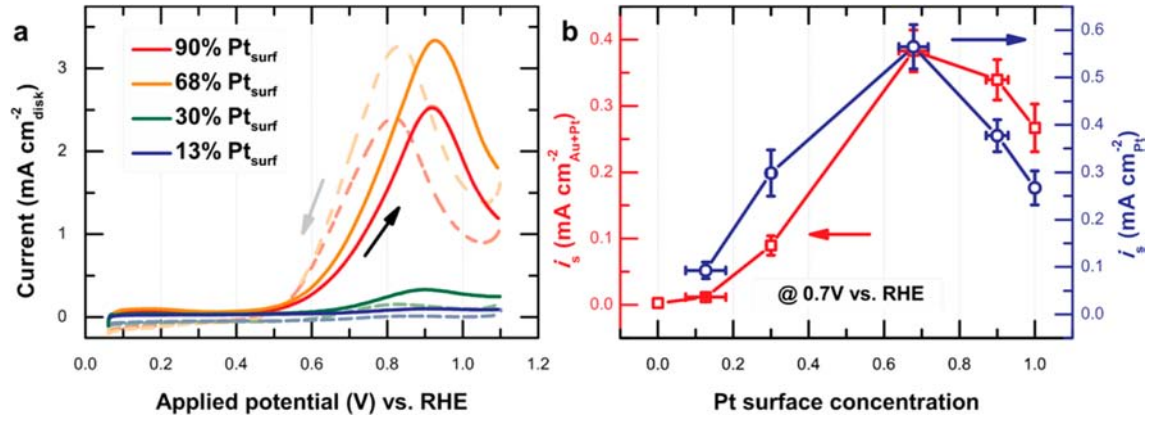

Figure 5. Activities of $Au_{0.5}Pt_{0.5}$ NPs at various surface compositions for the methanol electro-oxidation reaction (MOR). (a) The methanol electro-oxidation reaction (MOR) geometric current densities of $Au_{0.5}Pt_{0.5}$ NPs at various surface compositions in 0.1 M $HClO_4$ (at 50 mV s^{-1} scan rate, 0.018 mg_{metal} cm^{-2}_{disk} loading). (b) The specific MOR activities, i_s, of $Au_{0.5}Pt_{0.5}$ NPs (capacitance-corrected) normalized to either both Pt and Au surface area (red, left axis) or Pt surface area (blue, right axis) from the positive-going scan direction as a function of surface composition at 0.7 V vs RHE potential. The activity for 100% Pt was obtained from commercial Pt/C catalyst (Tanaka Kikinzoku). Error bars represent standard deviations of at least three independent measurements.

area of Pt and Au were measured as shown in Figure 5b and Supporting Information Figure S10. Like COR, the specific activities for MOR were found to greatly depend on the surface composition, exhibiting an increasing catalytic activity with increasing surface Au composition from the surface Pt-rich side, until reaching a maximum at the surface Pt concentration of ~70%, where the activity began to subsequently decrease with more surface Au on the surface Au-rich side (known as the "volcano relationship" in catalysis). Interestingly, $Au_{0.5}Pt_{0.5}$ nanoparticles at this optimum surface composition had higher specific activities than commercial Pt/C (both at ~3 and ~7 nm diameters, supplied by TKK and Johnson Matthey, respectively). The enhanced activity of these $Au_{0.5}Pt_{0.5}$ nanoparticles relative to Pt/C was also realized when normalized to the catalyst mass (Supporting Information Figure S11, compared only against ~7 nm commercial catalyst to avoid specific area difference), demonstrating the robustness of the catalytic enhancement in these nanomaterials. The MOR activity of the champion $Au_{0.5}Pt_{0.5}$ nanoparticles was found to be comparable to state-of-the-art Pt–Ru and Pt_3Sn nanoparticles with respect to both mass and surface area (Supporting Information, Table S2), although this was still lower than the result from the Pt–Ru extended surface.

To explain the volcano trend in the MOR activity, we first focus on the $Au_{0.5}Pt_{0.5}$ nanoparticles with Pt-enriched surface (the right side of the volcano), where MOR activity increases with Au addition. We attribute the enhancement on this branch to the modified Pt electronic structure[25] with weakened CO binding strength as proposed in the previous section. Specifically, the modified Pt electronic structure can more efficiently catalyze the COR, which is the rate-limiting step in the indirect mechanism of the MOR.[31,32] This hypothesis is congruent with previous reports that the electrochemical oxidation of methanol on Pt-based surfaces proceeds preferentially through the indirect pathway, where methanol undergoes dissociative adsorption and electrochemical dehydrogenation to form CO_{ad} ($CH_3OH \rightarrow CO_{ad} + 4H^+ + 4e^-$) before proceeding to the final step with the oxidation of the CO_{ad},[1,33] the latter of which is considered to be the rate-limiting step. This proposal agrees well with the observation

dx.doi.org/10.1021/ja402072r | J. Am. Chem. Soc. 2013, 135, 7985–7991

that the increase in the MOR activity with surface Pt enrichment (Figure 5) is concomitant with COR enhancement (Figure 4). We therefore propose that the origin of MOR enhancement can be attributed largely to the weakened CO binding on Pt, which increases the COR reactivity on $Au_{0.5}Pt_{0.5}$ nanoparticles. Within the framework of this hypothesis, Au again modifies the electronic structure of surface Pt, and therefore we normalize the MOR activity by the Pt surface area to more accurately assess the catalytic trend (Figure 5b, blue, right axis). With this normalization, the MOR activity monotonically increases with Au content on the volcano's right side (>50 atom % Pt), the same trend as what was observed in COR. This supports our hypothesis for the catalytic enhancement in the case of the Pt-rich surface $Au_{0.5}Pt_{0.5}$ nanoparticles.

To explain the activity trend of the $Au_{0.5}Pt_{0.5}$ nanoparticles with Au surface enrichment (the left side of the volcano), which has reduced MOR activity with increasing surface Au composition (both per total and Pt surface areas), we propose the rate-limiting step on this branch to be the dissociative adsorption/dehydrogenation of the methanol. With increasing Au surface enrichment, the probability of forming 3-fold Pt assembly on the surface[1,34] decreases, and thus the ability for the surface to dissociatively adsorb/dehydrogenate methanol decreases, resulting in the negative contribution to the MOR activity.

The optimum MOR activity occurs on $Au_{0.5}Pt_{0.5}$ nanoparticles with surface Pt composition of ~70 atom %, while the optimum MOR activity occurs at ~90 atom % Pt surface concentration[1,34] for Pt−Ru surfaces. This difference can be attributed to the dissimilar mechanisms responsible for the enhancement in the COR activity on $Au_{0.5}Pt_{0.5}$ nanoparticles and Pt−Ru and Pt_3Sn catalysts reported previously.[1,34,35] Unlike Au, Ru or Sn can promote water oxidation[36,37] to increase the availability of OH_{ad} at lower overpotential and consequently enhance the activity of COR via the bifunctional Langmuir−Hinshelwood mechanism (CO_{ad}-Pt + OH_{ad}-Ru → CO_2 + H^+ + e^-). Au, however, is much more inert, and therefore the catalytic reactions on the $Au_{0.5}Pt_{0.5}$ nanoparticles likely proceed only through Pt sites that have been modified by nearby and subsurface Au atoms, where the maximum COR activity might be obtained when Pt sites have attained the optimum CO binding. This is in contrast to in the case of Pt−Ru, where the optimum composition is reached when appropriate populations of CO_{Pt} and OH_{Ru} are formed.

We show that controlling the surface atomic concentration of Au on $Au_{0.5}Pt_{0.5}$ nanoparticles is immensely critical for the COR and MOR activities. The COR activity of the champion $Au_{0.5}Pt_{0.5}$ nanoparticles is also comparable to state-of-the-art Pt_3Sn nanoparticles with respect to both mass and surface area (Supporting Information Table S3), although it is important to recognize that this value is still lower than the result from the Pt_3Sn extended surface. In addition, our champion $Au_{0.5}Pt_{0.5}$ nanoparticle catalyst has significantly higher MOR activity than other Au−Pt catalysts reported previously (Supporting Information Table S2).[38−40] Even though Au alone is not active in water oxidation,[36] unlike Ru or Sn, it is interesting to note that the optimum MOR activities of $Au_{0.5}Pt_{0.5}$ nanoparticles are comparable to those of state-of-the-art MOR catalysts such as Pt−Ru and Pt_3Sn nanoparticles (Supporting Information Table S2). Our work demonstrates that electronic structure control by way of surface composition manipulation represents another avenue for designing a future generation of nanoparticle electrocatalyst. Further studies that combine the advantages from both the electronic effect (such as Au), as demonstrated in this work, and the classical bifunctional effect (such Ru or Sn) can be an interesting area for the design of highly active catalysts that promote the oxidation of small organic molecules.

■ CONCLUSION

We present a correlation between electrocatalytic activities and surface compositions of bimetallic nanoparticles. By manipulating and controlling the heat treatment conditions, we utilize surface energy as a means of selectively enriching either Pt or Au on the $Au_{0.5}Pt_{0.5}$/C nanoparticle catalysts. Our finding demonstrates that tuning the surface composition is critical to enhance the catalytic activity and that, without it, the as-measured catalytic activity may not be representative of the true catalytic potential of nanoparticles. The enhanced COR and MOR activities of $Au_{0.5}Pt_{0.5}$ can be attributed to the weakened CO binding on Pt in the presence of Au, where Au serves as an electronic modifier to reduce CO poisoning on Pt. Our finding reflects the critical importance of controlling surface composition for nanoparticle electrocatalysis, where we demonstrate the same bulk $Au_{0.5}Pt_{0.5}$ nanoparticles can have enhanced or reduced activities depending on the surface composition. This avenue of optimization must be integrated in the design of future highly active electrocatalysts.

■ ASSOCIATED CONTENT

Supporting Information

Details on specific heat treatment condition, surface area determination, and reaction order analysis. Particle size distribution of all Au−Pt particles, X-ray diffraction on all Au−Pt particles, details on surface area extraction from cyclic voltammograms, thermogravimetry of Au−Pt colloids, CO reaction order data for Au−Pt particles, CO stripping voltammetry of Au−Pt particles, additional STEM-EDS images, and activity comparison. This material is available free of charge via the Internet at http://pubs.acs.org.

■ AUTHOR INFORMATION

Corresponding Author

hubert.gasteiger@tum.de; schiffer@mit.edu; shaohorn@mit.edu

Present Addresses

[‖]Department of Chemistry, Technische Universität München, Lichtenbergstrasse 4, D 85747 Garching, Germany.

[#]MIT Lincoln Laboratory, 244 Wood St., Lexington, MA 02420.

[¶]Theory and Simulation of Materials, École Polytechnique Fédérale de Lausanne, 1015 Lausanne, Switzerland.

Author Contributions

[▽]These authors contributed equally.

Notes

The authors declare no competing financial interest.

■ ACKNOWLEDGMENTS

This work was supported in part by the MRSEC Program of the National Science Foundation under award number DMR 0819762, the DOE Hydrogen Initiative program under award number DE-FG02-05ER15728, and the DOE EERE award DE-EE0000458 via subcontract through General Motors. Microscopy work at Oak Ridge National Laboratory's High Temper-

ature Materials Laboratory was sponsored by the U.S. Department of Energy, Office of Energy Efficiency and Renewable Energy, Vehicle Technologies Program. J.S. was supported by the Chesonis Foundation Fellowship. The authors would like to thank Dr. Eva Mutoro for the help with the illustration.

REFERENCES

(1) Gasteiger, H. A.; Markovic, N.; Ross, P. N.; Cairns, E. J. *J. Phys. Chem.* **1993**, *97*, 12020.
(2) Stamenkovic, V. R.; Mun, B. S.; Arenz, M.; Mayrhofer, K. J. J.; Lucas, C. A.; Wang, G. F.; Ross, P. N.; Markovic, N. M. *Nat. Mater.* **2007**, *6*, 241.
(3) Gasteiger, H. A.; Markovic, N.; Ross, P. N.; Cairns, E. J. *J. Phys. Chem.* **1994**, *98*, 617.
(4) Norskov, J. K.; Bligaard, T.; Rossmeisl, J.; Christensen, C. H. *Nature Chem.* **2009**, *1*, 37.
(5) Yu, W.; Porosoff, M. D.; Chen, J. G. *Chem. Rev.* **2012**, *112*, 5780.
(6) Tian, N.; Zhou, Z. Y.; Sun, S. G.; Ding, Y.; Wang, Z. L. *Science* **2007**, *316*, 732.
(7) Chen, S.; Sheng, W. C.; Yabuuchi, N.; Ferreira, P. J.; Allard, L. F.; Shao-Horn, Y. *J. Phys. Chem. C* **2009**, *113*, 1109.
(8) Mayrhofer, K. J. J.; Juhart, V.; Hartl, K.; Hanzlik, M.; Arenz, M. *Angew. Chem., Int. Ed.* **2009**, *48*, 3529.
(9) Tao, F.; Grass, M. E.; Zhang, Y. W.; Butcher, D. R.; Renzas, J. R.; Liu, Z.; Chung, J. Y.; Mun, B. S.; Salmeron, M.; Somorjai, G. A. *Science* **2008**, *322*, 932.
(10) Kitagawa, H.; Kobayashi, H.; Yamauchi, M.; Kubota, Y.; Kato, K.; Takata, M. *J. Am. Chem. Soc.* **2010**, *132*, 5576.
(11) Yang, H. *Angew. Chem., Int. Ed.* **2011**, *50*, 2674.
(12) Wang, D. L.; Xin, H. L.; Wang, H. S.; Yu, Y. C.; Rus, E.; Muller, D. A.; DiSalvo, F. J.; Abruna, H. D. *Chem. Mater.* **2012**, *24*, 2274.
(13) Peng, Z. M.; Yang, H. *Nano Res.* **2009**, *2*, 406.
(14) Mazumder, V.; Chi, M. F.; More, K. L.; Sun, S. H. *Angew. Chem., Int. Ed.* **2010**, *49*, 9368.
(15) Hartl, K.; Mayrhofer, K. J. J.; Lopez, M.; Goia, D.; Arenz, M. *Electrochem. Commun.* **2010**, *12*, 1487.
(16) Zhang, J.; Sasaki, K.; Sutter, E.; Adzic, R. R. *Science* **2007**, *315*, 220.
(17) Luo, J.; Njoki, P. N.; Lin, Y.; Mott, D.; Wang, L. Y.; Zhong, C. J. *Langmuir* **2006**, *22*, 2892.
(18) Luo, J.; Wang, L.; Mott, D.; Njoki, P. N.; Lin, Y.; He, T.; Xu, Z.; Wanjana, B. N.; Lim, I. I. S.; Zhong, C. J. *Adv. Mater.* **2008**, *20*, 4342.
(19) Braidy, N.; Purdy, G. R.; Botton, G. A. *Acta Mater.* **2008**, *56*, 5972.
(20) Needs, R. J.; Mansfield, M. *J. Phys. Condens. Matter* **1989**, *1*, 7555.
(21) Hammer, B.; Norskov, J. K. *Adv. Catal.* **2000**, *45*, 71.
(22) Carlton, C. E.; Chen, S.; Ferreira, P. J.; Allard, L. F.; Shao-Horn, Y. *J. Phys. Chem. Lett.* **2012**, *3*, 161.
(23) Xu, Z. C.; Carlton, C. E.; Allard, L. F.; Shao-Horn, Y.; Hamad-Schifferli, K. *J. Phys. Chem. Lett.* **2010**, *1*, 2514.
(24) Greeley, J.; Norskov, J. K. *Electrochim. Acta* **2007**, *52*, 5829.
(25) Pedersen, M. O.; Helveg, S.; Ruban, A.; Stensgaard, I.; Laegsgaard, E.; Norskov, J. K.; Besenbacher, F. *Surf. Sci.* **1999**, *426*, 395.
(26) Eyrich, M.; Diemant, T.; Hartmann, H.; Bansmann, J.; Behm, R. J. *J. Phys. Chem. C* **2012**, *116*, 11154.
(27) Vandertoorn, L. J.; Tiedema, T. J. *Acta Metallurgica* **1960**, *8*, 711.
(28) Schmidt, T. J.; Gasteiger, H. A.; Behm, R. J. *J. Electrochem. Soc.* **1999**, *146*, 1296.
(29) Kim, J.; Samano, E.; Koel, B. E. *J. Phys. Chem. B* **2006**, *110*, 17512.
(30) Ren, H.; Humbert, M. P.; Menning, C. A.; Chen, J. G.; Shu, Y. Y.; Singh, U. G.; Cheng, W. C. *Appl. Catal., A* **2010**, *375*, 303.
(31) Lee, S. W.; Chen, S. O.; Sheng, W. C.; Yabuuchi, N.; Kim, Y. T.; Mitani, T.; Vescovo, E.; Shao-Horn, Y. *J. Am. Chem. Soc.* **2009**, *131*, 15669.
(32) Lebedeva, N. P.; Koper, M. T. M.; Feliu, J. M.; van Santen, R. A. *J. Phys. Chem. B* **2002**, *106*, 12938.
(33) Lin, W. F.; Iwasita, T.; Vielstich, W. *J. Phys. Chem. B* **1999**, *103*, 3250.
(34) Gasteiger, H. A.; Markovic, N.; Ross, P. N.; Cairns, E. J. *J. Electrochem. Soc.* **1994**, *141*, 1795.
(35) Gasteiger, H. A.; Markovic, N. M.; Ross, P. N. *J. Phys. Chem.* **1995**, *99*, 8945.
(36) Borkowska, Z.; Tymosiak-Zielinska, A.; Shul, G. *Electrochim. Acta* **2004**, *49*, 1209.
(37) House, C. I.; Kelsall, G. H. *Electrochim. Acta* **1984**, *29*, 1459.
(38) Lin, Z. H.; Shih, Z. Y.; Tsai, H. Y.; Chang, H. T. *Green Chem.* **2011**, *13*, 1029.
(39) Ding, Y.; Ge, X. B.; Wang, R. Y.; Liu, P. P. *Chem. Mater.* **2007**, *19*, 5827.
(40) Luo, J.; Maye, M. M.; Kariuki, N. N.; Wang, L. Y.; Njoki, P.; Lin, Y.; Schadt, M.; Naslund, H. R.; Zhong, C. J. *Catal. Today* **2005**, *99*, 291.